

Mid-infrared, H α and radio continuum images of an unusual H II region, G308.70 + 0.60

Martin Cohen,^{1*} Anne J. Green,² Quentin A. Parker,^{3,4}
Stacy Mader⁵ and Russell D. Cannon⁴

¹Radio Astronomy Laboratory, University of California, Berkeley, CA 94720, USA

²School of Physics, University of Sydney, NSW 2006, Australia

³Department of Physics, Macquarie University, NSW 2109, Australia

⁴Anglo-Australian Observatory, PO Box 296, Epping, NSW 2121, Australia

⁵Australia Telescope National Facility, CSIRO, PO Box 276, Parkes, NSW 2870, Australia

Accepted 2002 June 12. Received 2002 May 3; in original form 2002 January 24

ABSTRACT

We report on a multi-wavelength study of images in the mid-infrared (MIR), H α and radio continuum of an unusual H II region, G308.70 + 0.60. Using images from the *Midcourse Space Experiment (MSX)* between 8.3 and 21.3 μm , from the AAO/UK Schmidt Telescope (UKST) deep, high-resolution, H α survey of the plane, and from the Molonglo Observatory Synthesis Telescope (MOST) Galactic plane survey in the radio continuum at 843 MHz, we have investigated the morphology of the nebula and propose that there is an interaction between the interstellar medium and a star lying inside the large nebular bubble. Secondary star formation appears to have occurred in several places on the dense rim of the bubble. In one such site, this has resulted in a luminous MIR double star, situated within the rim of the nebular ring, that has created its own local bubble.

Key words: stars: formation – H II regions – ISM: structure – infrared: ISM – infrared: stars – radio continuum: ISM.

1 INTRODUCTION

The intercomparison of multi-wavelength imaging surveys highlights different aspects and components of the interstellar medium (ISM). In this paper we investigate a peculiar object in the southern Galactic plane, through direct comparison of mid-infrared (MIR) images, provided by the *Midcourse Space Experiment (MSX)* (Mill et al. 1994); narrow-band H α images drawn from the AAO/UKST H α survey (Parker, Phillips & Morgan 1999); and radio continuum data, from the 843-MHz Molonglo Galactic plane Surveys, MGPS1 (Green et al. 1999) and MGPS2 (Green 1999). From this initial study we have evolved a strategy for using these unique panoramic surveys to intercompare a variety of structures and features over a wide range of spatial scales, from tens of degrees down to subarcmin. By directly overlaying images from each survey, the triple comparison offers the prospect of examining the morphology and different physical processes inherent in the interactions between stars and the ISM. Here we concentrate on such a multi-wavelength study of the unusual H II region G308.70 + 0.60. We characterize it as unusual because it has an essentially ring-like morphology yet there is a dominant bright object on the rim, rather than in the interior, and there are several nebular protuberances that emerge from the rim.

1.1 Previous radio observations of G308.70 + 0.60

Our interest in the H II region, G308.70 + 0.60, first came from an inspection of the MGPS2 images, which show a striking similarity to the odd Y-shaped mid-infrared structure. The object has been classified as a thermal source for more than three decades. The earliest mention of this area was by Wilson et al. (1970) who detected the H109 α radio recombination line from ($l, b = 308.73, +0.57$) at an LSR velocity of $-52 \pm 6 \text{ km s}^{-1}$ in a 4-arcmin beam. Bronfman, Nyman & May (1996) measured the CS 2-1 line from (308.746, +0.549) at an LSR velocity of -48 km s^{-1} . In a search of several hundred *IRAS* sources satisfying the *IRAS* colour criteria for ultracompact H II regions defined by Wood & Churchwell (1989), Van Der Walt, Gaylard & MacLeod (1995) discovered a 6.7-GHz methanol maser using a 7-arcmin beam in the velocity range -52 to -40 km s^{-1} at (308.74, +0.55), corresponding to *IRAS* 13 374–6130 (308.75, +0.55). Note that all these slightly different positions are consistent given the respective low spatial resolutions of the various instruments. These three independent velocity determinations from the region are consistent with a value around -49 km s^{-1} , from which we derive a distance of $\sim 5.3 \pm 0.4 \text{ kpc}$, using the rotation curve of Fich, Blitz & Stark (1989). There is no distance ambiguity in this estimate because the velocity of the sources corresponds to the tangent point for this longitude.

*E-mail: mcohen@astro.berkeley.edu

Wilson et al. (1970) also tabulated a second H II region at (308.65, +0.59), with LSR velocity $-46 \pm 4 \text{ km s}^{-1}$, while Caswell & Haynes (1987) observed an almost identical position (308.65, +0.58) and measured an LSR velocity of -50 km s^{-1} from the average of the H109 α and H110 α lines. The similarity of these velocities to those of the brighter H II region suggests that both regions are at the same distance along our line-of-sight. The Parkes–MIT–NRAO (PMN) survey by Wright et al. (1994) at 4.85-GHz produced a spatially filtered catalogue of point sources with 4.2-arcmin resolution. PMN J1340-6144 corresponds to the radio-bright western rim of the ring-like 8.3- μm morphology that we describe below, but their measurements indicate that this is not an isolated, unresolved Gaussian source. Our results indicate that G308.70 + 0.60 is a complex ionized structure with several associated H II regions, in which case the H109 α and PMN multiple sources show the blending of emission from these H II regions.

In the next section we give a brief description of the three surveys used, and present the images. The results of the multi-wavelength comparison are given in Section 3, followed by spectroscopy in the red band covering H α , [N II], [S II], and [A II] nebular lines in Section 4. Section 5 describes our analysis of H I and ^{12}CO data cubes of the region. Section 6 proposes an explanation for this unusual system and our conclusions are given in Section 7.

2 THE SURVEYS

2.1 MSX: mid-infrared

Multiband MIR panoramic surveys covering several hundred square degrees with spatial resolution superior to 30 arcsec have not been available until recently. Details of the *MSX* infrared instruments and the processing of their data products for the Galactic plane can be found in Price et al. (2001) and Egan et al. (1999). *MSX* surveyed the entire Galactic plane during 1996–1997, within the range $|b| \leq 5^\circ$, simultaneously at six wavelengths from 4.2 to 21 μm . Full-resolution *MSX* images are distributed by IPAC,¹ for community access. These images have 20-arcsec resolution, with 6-arcsec pixels and dimensions of roughly $1.6 \times 1.6 \text{ deg}^2$. SPIRIT-III (SPatial InfraRed Imaging Telescope) is the MIR instrument on *MSX*, which covered six wavelength bands detecting emission from molecular gas, warm ($\sim 300 \text{ K}$) and cool ($\sim 150 \text{ K}$) dust grains. For the study of the Galactic plane, four of these bands are important (those with isophotal wavelengths of 8.3, 12.1, 14.6, 21.3 μm).

These four *MSX* bands predominantly probe two basic physical mechanisms, namely fluorescent polycyclic aromatic hydrocarbon (PAH) emission and thermal emission by dust. PAH discrete emission bands and extended plateaus of emission occur prominently in the 8.3- and 12.1- μm bands, and very weakly in the 14.6- μm band. Hence, similar structures are expected to be detected in at least two of these three bands. However, distinctly different morphologies will be seen in the longest wavelength band (21.3 μm), which is likely to detect even heavily obscured exciting stars of ionized regions, and cool dust heated by starlight or resonantly trapped Lyman- α photons. The 8.3- μm band offers the deepest *MSX* coverage of the plane partly because of the responsiveness of the material used for these detectors, and partly because all eight columns of pixels in this radiometer were read out (as opposed to the other bands for which only either 2 or 4 columns were read). The four bands used

¹ The Infrared Processing and Analysis Centre in Pasadena, California distributes *MSX* images through the Infrared Science Archive at <http://irsa.ipac.caltech.edu/>.

in this paper suffer minimally from extinction, with values of A_λ of 0.037, 0.020, 0.007, and 0.004 mag kpc^{-1} , respectively.

2.2 UKST H α

The AAO/UKST has made an H α survey (Parker & Phillips) of the Southern Galactic plane and Magellanic Clouds using a high-quality 1 per cent bandwidth, single-element, interference filter centred near H α (Parker & Bland-Hawthorn 1998) and high-resolution Tech–Pan film (Parker & Malin 1999). The H α survey uses 3-h exposures to achieve limiting magnitudes for unresolved sources equivalent to $R \sim 20.5$, although the completeness falls beyond $R = 20$ mag. It covers the entire southern Milky Way for $|b| \leq 10^\circ$, based on a grid of 5:5 diameter circular regions with centres 4° apart, and has an inherent resolution of about 2 arcsec. Details of the H α survey can be found at <http://www.roe.ac.uk/wfau/halpha/halpha.html>. The survey has a coverage, resolution and sensitivity which CCDs cannot yet match, although interstellar extinction is a limiting factor. The SuperCOSMOS plate measuring machine at the Royal Observatory Edinburgh (Miller et al. 1992) is being used to scan the H α films at 10- μm (0.67 arcsec) resolution. The optical images presented here are from SuperCOSMOS digital scans of the original H α survey films and of the *R*-band and *I*-band Schmidt plates.

2.3 MGPS2 – 843-MHz radio continuum

The Molonglo Observatory Synthesis Telescope (MOST) is an east–west array operating in the radio continuum at 843 MHz with a resolution of $(43 \times 43 \text{ arcsec}^2) \text{cosec}|\delta|$ (Mills 1981; Robertson 1991). MGPS1 data are available in the form of $3 \times 3 \text{ deg}^2$ fields (Green et al. 1999). In this paper, a mosaic was created from observations made as part of the second epoch survey, MGPS2 (Green 1999), which uses the MOST in its upgraded wide-field mode (Bock, Large & Sadler 1999). MGPS2 is part of the Sydney University Molonglo Sky Survey (SUMSS), currently in progress. The new observations have lower levels of artefacts and have a 1σ sensitivity of 1–2 mJy beam^{-1} for a complete 12 h synthesis.

2.4 Multi-wavelength images of G308.70 + 0.60

2.4.1 Mid-infrared

We made 1×2 mosaics of the 8.3-, 12.1-, 14.6-, and 21.3- μm standard, $1.6 \times 1.6 \text{ deg}^2$ *MSX* images, to cover G308.70 + 0.60 and the low-surface-brightness northern extension of the MIR nebulosity (Figs 1a–d). Fig. 1(a) illustrates the uneven, filamentary character of the MIR photodissociation region (PDR) around this object, as seen by Cohen & Green (2001) for several H II regions in their comparison of MIR and radio continuum images in the Galactic plane. This same character is also obvious in Fig. 1(b) because both the 8.3- and 12.1- μm bands are sensitive to the PAH emission in PDRs. By contrast, at 14.6 and 21.3 μm , the structure has changed to one dominated by thermal emission by cool dust grains, and the large ring nebula is invisible at 21.3 μm .

2.4.2 H α

G308.70+0.60 appears on the UKST H α exposure HA18450, taken on 1999 June 19, and centred at RA (B1950) $13^{\text{h}} 20^{\text{m}}$, Dec. (B1950) -60° , which corresponds to $l = 307^\circ$, $b = +2.5$. Fig. 2 gives the grey-scale 2160×2160 pixel image, reproduced from the 10- μm

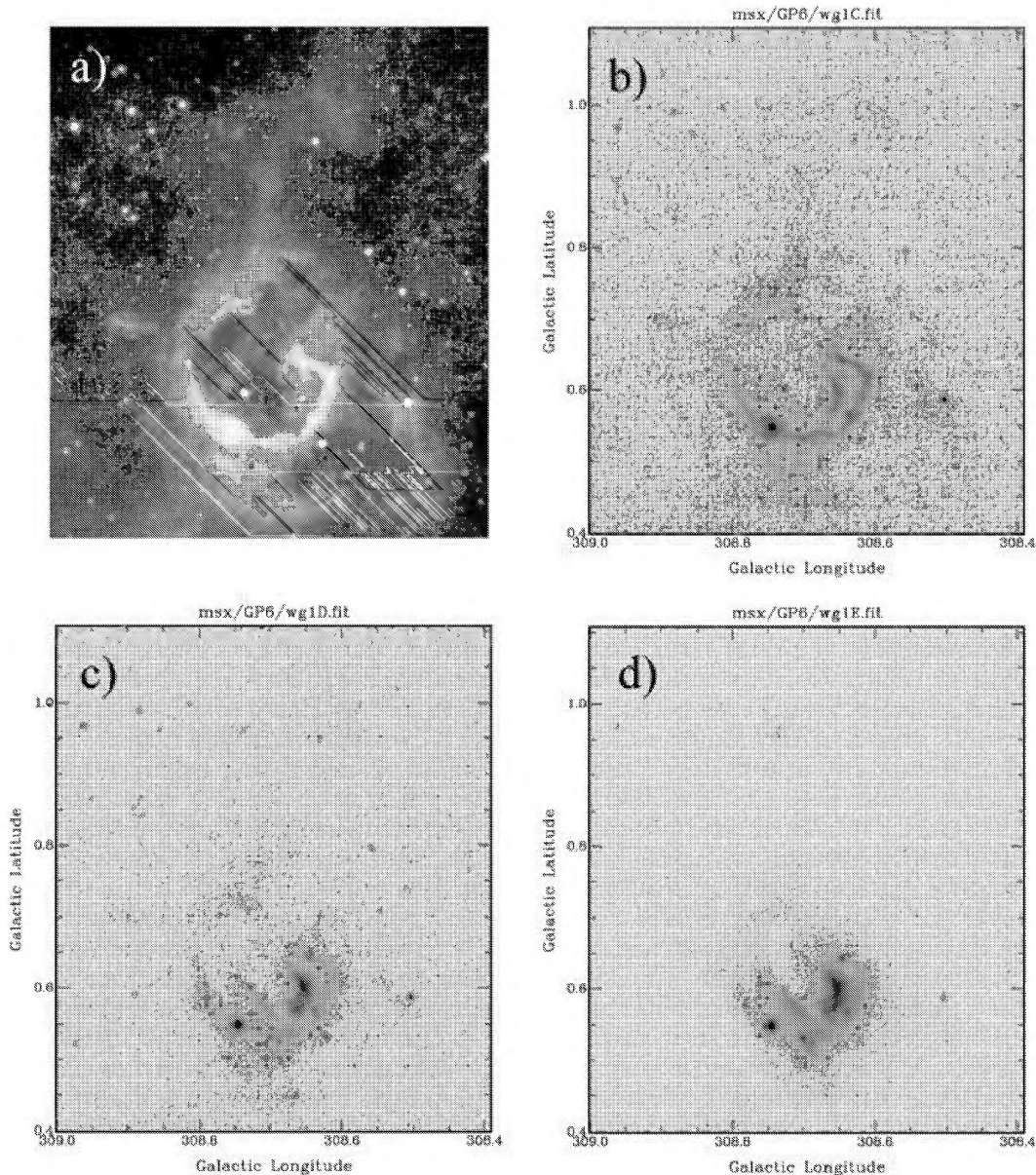


Figure 1. Logarithmic intensity plots of G308.70 + 0.60 at (a) 8.3, (b) 12.1, (c) 14.6 and (d) 21.3 μm . That at 8.3 μm represents a negative image of G308.70 + 0.60 and its environs after contrast enhancement and unsharp masking. The other three wavelengths are represented by simple grey-scale images. The maximum and minimum radiance values represented in (a) by white and black pixels, respectively, are 1.1×10^{-4} and $6.0 \times 10^{-7} \text{ W m}^{-2} \text{ sr}^{-1}$. The minimum and maximum radiance values represented in the grey-scale images (by white and black pixels, respectively) are: (b) zero and 3.1×10^{-5} ; (c) zero and 2.9×10^{-5} ; (d) zero and $8.8 \times 10^{-5} \text{ W m}^{-2} \text{ sr}^{-1}$.

pixel (0.67 arcsec) resolution SuperCOSMOS data, and overlaid by *MSX* 8.3- μm contours. The overall morphologies in the $\text{H}\alpha$ map of ionized gas and the overlaid *MSX* 8- μm emission associated with the outer PDR (Fig. 2) are similar. Significant and localized optical extinction by dust is clearly evident and compares favourably with pale areas in the *MSX* images in Fig. 1.

2.4.3 Radio continuum

Fig. 3 overlays 843-MHz contours on the grey-scale image of G308.70 + 0.60 from the $\text{H}\alpha$ survey full-resolution exposure. The spatially integrated ratio of flux densities for the entire major ring

structure of G308.70 + 0.60, $F_{8.3\mu\text{m}}/S_{843\text{MHz}}$ (after correction for extraneous point sources and local background), is ~ 40 , somewhat higher than the median of 24 found by Cohen & Green (2001), but the semi-interquartile range these authors found was nine, and the distribution had a significant spread (six to 73). Therefore, the major ring is consistent with being due to thermal emission. Fig. 4 illustrates the close association between ionized gas (from both the $\text{H}\alpha$ and 843-MHz continuum emission) and the likely PDR delineated by the MIR images (particularly at 8.3 μm) which show faint emission beyond the ionized gas.

The radio continuum image of the region from MGPS2 alone appears in Fig. 5 as a logarithmic plot to show the dominant radio

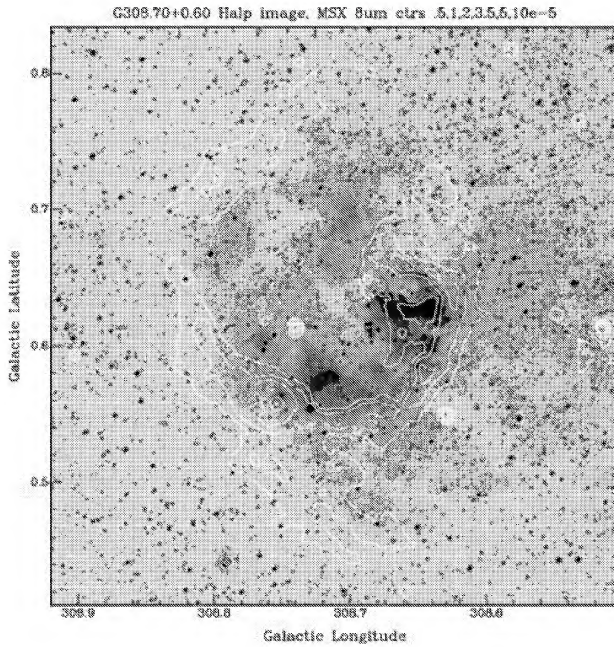


Figure 2. An image of G308.70 + 0.60 digitized from the H α exposure, HA18450; it is 0.4×0.4 deg 2 . North is up and east to the left throughout. No calibrated intensity scale is yet available for these data. The H α image is overlaid by white contours of 8.3- μ m emission for values of 0.4, 0.6, 1, 2, 3.5, 5, 10×10^{-5} W m $^{-2}$ sr $^{-1}$.

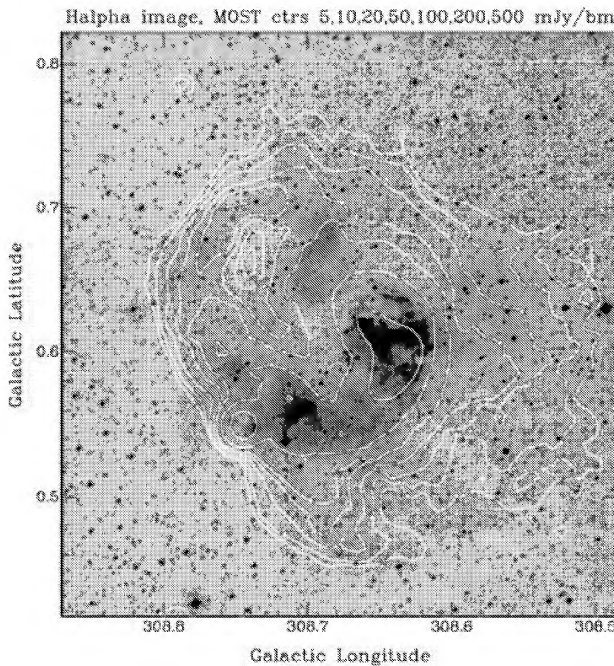


Figure 3. As Fig. 2, but overlaid by white contours of 843-MHz emission for values of 5, 10, 20, 50, 100, 200, 500 mJy beam $^{-1}$.

brightness of the source near the south-east rim of the partial bubble. Linear intensity plots are used when weaker features, for example the western part of the ring, are being studied. The dynamic range of the MOST image is $\sim 200 : 1$. Logarithmic and linear plots have been used with the MIR images in similar fashion.

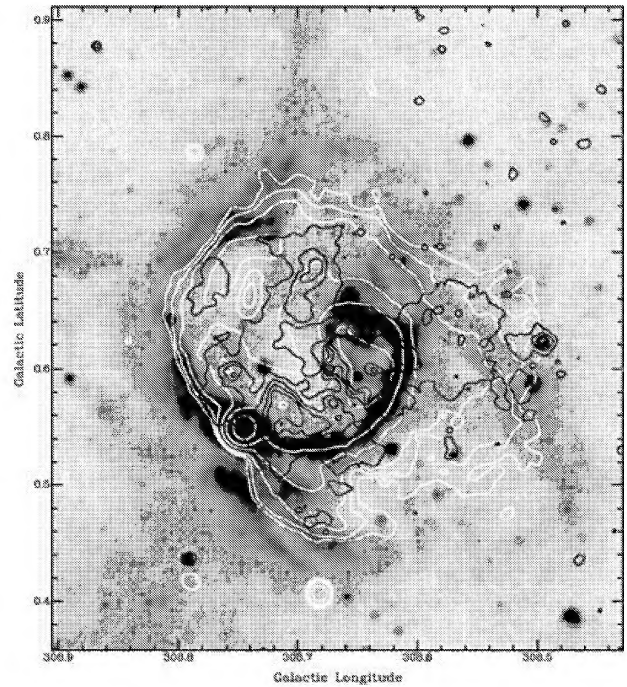


Figure 4. Linear, grey-scale image at 8.3 μ m of G308.70 + 0.60 overlaid by 843-MHz (white) contours for values of 5, 10, 20, 50, 100, 200 mJy beam $^{-1}$ and H α (black) contours at levels of 4000, 5000, 6000, 7000, 8000 (in arbitrary SuperCOSMOS units).

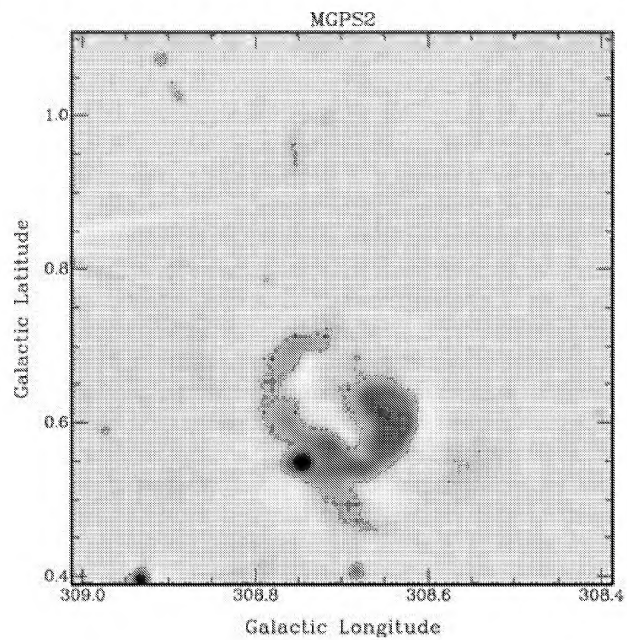


Figure 5. Logarithmic intensity plot of G308.70 + 0.60 from MGPS2 at 843 MHz. Minimum and maximum radiance values shown in this image are -27 and 338 mJy beam $^{-1}$, respectively, corresponding to white and black pixels.

3 MULTI-WAVELENGTH COMPARISON

Below we make a detailed multi-wavelength comparison of the H II region investigating, in particular, an intriguing embedded feature of the south-eastern rim of the bubble and other salient structures.

3.1 IRAS 13374 – 6130: the source on the south-east rim

The source IRAS 13374–6130, at (308.75,0.55) lies on the south-east rim of the overall structure and is bright in all *MSX* bands, with a clear counterpart in the MOST data. Images at MIR, radio, and optical wavelengths are compared in Fig. 4, in which the grey-scale image at 8.3 μm is overlaid by 843-MHz radio continuum (white contours) and $H\alpha$ data (black contours). The observed *MSX* colour indices of this object, $[12.1]-[21.3] = 2.68$, and $[14.6]-[21.3] = 2.05$, are in fair accord with those expected for an H II region (2.71 and 1.77, respectively, defined by using the wavelength-flexible ‘SKY’ model (Cohen 1994) of the point sky to generate tables of *MSX* absolute magnitudes for 87 types of MIR celestial source. The location of the ionized gas is well-shown by both the radio continuum and $H\alpha$ images, although the optical image clearly suffers significant extinction, presumably from a combination of foreground interstellar reddening and from material associated with the nebula itself. The presence of the local extinction can be inferred both from the sharply defined inner edge of the 8.3- μm emission interior to the broken ring, and from the fact that the $H\alpha$ peak near the star does not actually occur at the position of the *IRAS* source, as deduced from the 21.3- μm (Fig. 1d) and radio (Fig. 5) peaks. In fact, the $H\alpha$ bright spot is offset by 33 arcsec from this source.

A particularly interesting feature from the 8.3- μm image is IRAS 13374–6130 itself, which is seen to consist of a point-like object and a surrounding, almost complete, circular shell straddling the rim (Fig. 6). This shell is best-defined at 8.3 μm , progressively fainter at 12.1 and 14.6 μm , and has essentially vanished by 21.3 μm (Fig. 7). The compact central source is seen as a clear double at 21.3 μm , and has a fainter component in the other MIR images. From the *MSX* images, we have extracted the flux densities of this faint component. It is difficult at 8.3 and 12.1 μm to avoid contamination by the much brighter western component, but the 14.6- and 21.3- μm flux densities suggest a spectral energy distribution (SED) of an object with colour temperature of only 115 K. The *MSX* colours of this source, and the spatially integrated value of $F_{8.3\mu\text{m}}/S_{843\text{MHz}}$, 21, are

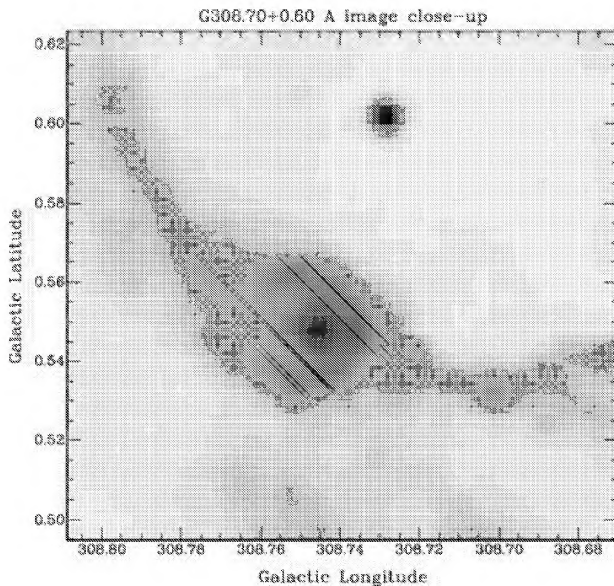


Figure 6. Linear, grey-scale, 8.3- μm image G308.70 + 0.60 showing the double star lying within a circular nebula. At 8.3 μm , the eastward extension of the bright star in the nebula is all that is seen of the companion.

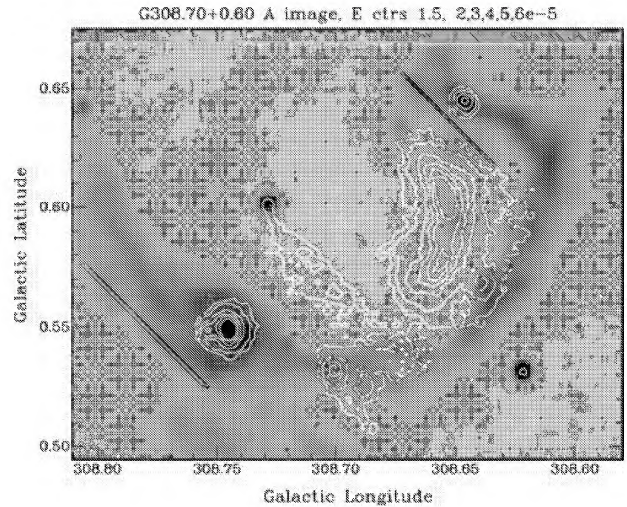


Figure 7. Linear, grey-scale, 8.3- μm image of G308.70 + 0.60 overlaid by 21.3- μm white contours for values of 1.5, 2, 3, 4, 5, 6 $\times 10^{-5} \text{ W m}^{-2} \text{ sr}^{-1}$. The eastern companion of the star in the ring nebula is shown in the white contours. Also note the intriguing quasi-linear ‘pointer’ that seems to link an interior 8.3- μm point source to the southern rim of the ring.

also consistent with a compact H II region [the median value of this ratio obtained by Cohen & Green (2001) was 24].

IRAS 13374–6130 is the brightest MIR object in this field, with coincident peaks in radio continuum, 8.3- and 21.3- μm emission at (308.745, +0.548), suggesting the presence of a small ionized region on the rim of the nebular ring, well shown by SUMSS too (Fig. 5). The character of this source is confirmed by the *IRAS* Low Resolution Spectrometer (LRS) data for IRAS 13374–6130 from the data base maintained at the NASA–Ames Research Centre. The LRS spectrum was recalibrated, as described by Cohen, Walker & Witteborn (1992). Fig. 8 illustrates the spectrum, with $\pm 1\sigma$ uncertainties at each wavelength, normalized to an *IRAS* 12- μm flux density of 27.89 Jy, based on the Faint Source Catalog Rejects (FSCR) for source Z13374–6130 (the *IRAS* Point Source Catalog contains

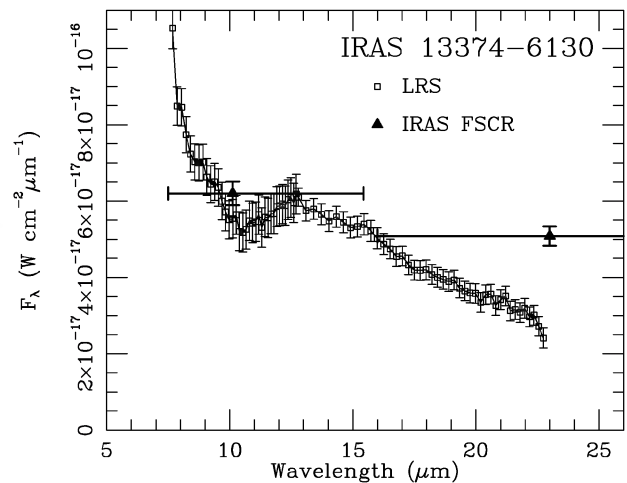


Figure 8. The recalibrated MIR spectrum of IRAS 13374–6130 with $\pm 1\sigma$ uncertainties. Also plotted are the *IRAS* flux densities (filled triangles) from the Faint Source Reject Catalog.

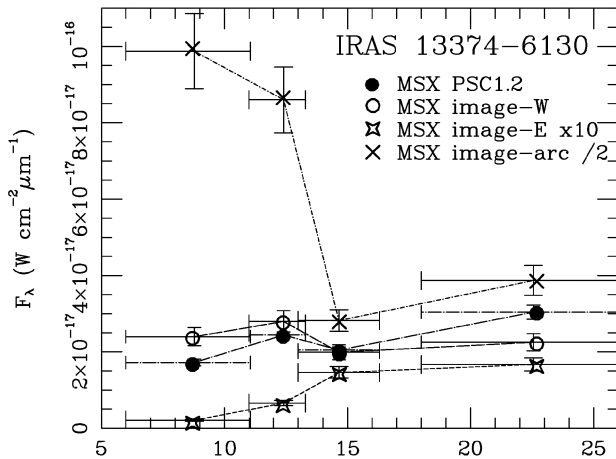


Figure 9. The flux densities from the *MSX* PSC1.2 (filled symbols), and the results of spatially integrating the two components of the double source and the small arc nebula in the *MSX* images. Figs 8 and 9 have identical axes for ease of comparison.

only an upper limit for the 12- μm flux density, which is a prerequisite for calibration of an LRS spectrum: Cohen et al. 1992).

The LRS spectrum suggests an H II region (see Volk & Cohen 1989), with significant 9.7- μm silicate absorption. We estimate $\tau(9.7 \mu\text{m}) \sim 0.34 \pm 0.04$, whence $A_v \sim 6.3 \pm 0.3$, using the Roche & Aitken (1984) observed ratio of $A_v/\tau(9.7 \mu\text{m}) = 18.5 \pm 1.5$. This is consistent with a region of secondary star formation on the rim of G308.70 + 0.60, observed through heavy local obscuration. Also plotted, at their correct isophotal wavelengths for this spectrum, are the flux densities at 12 and 25 μm from the *IRAS* FSCR (Fig. 8), and those derived by spatial integration of the *MSX* images. The comparison between the *IRAS* (Fig. 8) and *MSX* (Fig. 9) Point Source Catalog flux densities indicates the extended nature of the *IRAS* source because the *IRAS* beams include both components of the double and portions of the small nebulous arc, and these are substantially above the *MSX* PSC1.2 flux densities. To distinguish the much fainter eastern object from its bright neighbour, we have removed the latter by fitting a two-dimensional Gaussian to it. The SEDs of the bright (west: open circles, scaled $\times 10$) and faint (east: open stars) components of the double source within *IRAS* 13 374–6130 are shown in Fig. 9. These have much redder SEDs than the LRS suggests because of the inclusion of considerable diffuse PAH emission within the large *IRAS* LRS detectors. For comparison, the spatially integrated SED of the small arc nebula (crosses: scaled $\times 0.5$) is plotted. This nebular SED is dominated by PAH emission in the 8.3 and 12.1- μm bands, consistent with its very ‘blue’ appearance (Fig. 1).

For the *IRAS* flux densities of *IRAS* 13 374–6130 (the double star and part of the arc nebula) and the *MSX* flux densities of the arc nebula (Fig. 7) alone, we attribute the 8.3- μm emission, and a portion of that detected at 12.1 μm , to PAH bands. The residual 12.1- μm contribution from the two MIR sources, and the corresponding 14.6 and 21.3- μm emission, are consistent with radiation from optically thick dust grains at ~ 95 K. The small surrounding arc of nebulosity has a temperature ~ 70 K, rather poorly defined solely on the basis of its 14.6 and 21.3- μm emission. Estimates of the minimum bolometric luminosity from the elements of *IRAS* 13 374–6130, based upon combining the energy distributions observed by *MSX* with a lower-bound extrapolation beyond the longest observed wavelength (Cohen 1973; Chavarria 1981) are: 10 000 L_\odot (the bright west-

ern star); 500 L_\odot (the fainter, but much redder, eastern object); and 30 000 L_\odot (the arc nebula). These components total at least 40 000 L_\odot . The same method, applied to the larger beam *IRAS* FSCR observations that extend to 60 μm , yields at least 69 000 L_\odot . These estimates implicate at least one high-mass star, probably with $\sim 20 M_\odot$, consistent with the presence of the methanol masers, which are found at the emergence of an ultracompact H II region but rarely survive these earliest phases of high-mass star formation (Caswell 2001).

Caswell (private communication) has refined the location of the methanol maser in this region using the Australia Telescope Compact Array with 2-arcsec resolution. He has confirmed the presence of three methanol peaks in the velocity range found by Van Der Walt et al. (1995) but has localized all three to within a 1 arcsec vicinity of (308.754, +0.549). This precision suffices to associate the masers with the faint, very red, eastern component of the MIR double star, while the *IRAS* source corresponds primarily to the bright western component. Given the great redness of the eastern source, it is quite possible that it contributes significantly to the 60 and 100- μm *IRAS* flux densities, so that the proportions of the total luminosity assigned above to the eastern and western components are incorrect. However, the *IRAS* FSCR data still provide a plausible upper limit to the luminosity of everything within ‘*IRAS* 13 374–6130.’

3.2 The major ring of G308.70 + 0.60

G308.70 + 0.60 resembles a bubble blown by an exciting star. The overall morphology of G308.70 + 0.60 conforms most closely to the ‘cometary’ shape for ultracompact H II regions, described by Wood & Churchwell (1989). Such objects inevitably have their exciting stars close to the foci of these generally parabolic rims. The term ‘cometary’ was applied to larger H II regions by Reid & Ho (1995), using G34.26+0.15 as the paradigm. Its macroscopic morphology (at comparable resolution) is much more complex than that of G308.70+0.60, yet the exciting star in G34.26+0.15 (its location inferred from the coincident 8.3 and 21.3- μm peaks) is definitely located *inside* that nebular rim. By implication, we cannot plausibly identify the star on the rim (*IRAS* 13 374–6130) as responsible for creating the large bubble of G308.70 + 0.60. If cometary H II regions result from the bowshocks caused by supersonic motions of the exciting stars through the ISM (e.g. Van Buren, Noriega-Crespo & Dgani 1995), then G308.70 + 0.60 would have to lie in ambient gas that is exceptionally dense to the south-east in order for the star itself to lie on the parabolic rim.

A more likely candidate for the exciting star of the major ring is proposed in Section 6.

3.3 Other associated structures

It is possible to differentiate between those parts of the MIR images that emit in the PAH bands and those that produce continuum emission by comparing the *MSX* images in the four wavelength bands, as shown in Figs 10(a), (b) and (c). These compare the 12.1, 14.6- and 21.3- μm images (respectively) in white contours with the 8.3- μm linear grey-scale image of G308.70 + 0.60. Several features can be readily identified: stars (bright unresolved sources in all four bands); compact H II regions, e.g. the brightest source on the nebular rim which is extended at all four wavelengths; diffuse PAH emission from the nebular ring which is morphologically identical at 8.3, 12.1 and 14.6 μm ; and cool, dust continuum emission from structures which are similar at 12.1, 14.6 and 21.3 μm but not seen at 8.3 μm (see below).

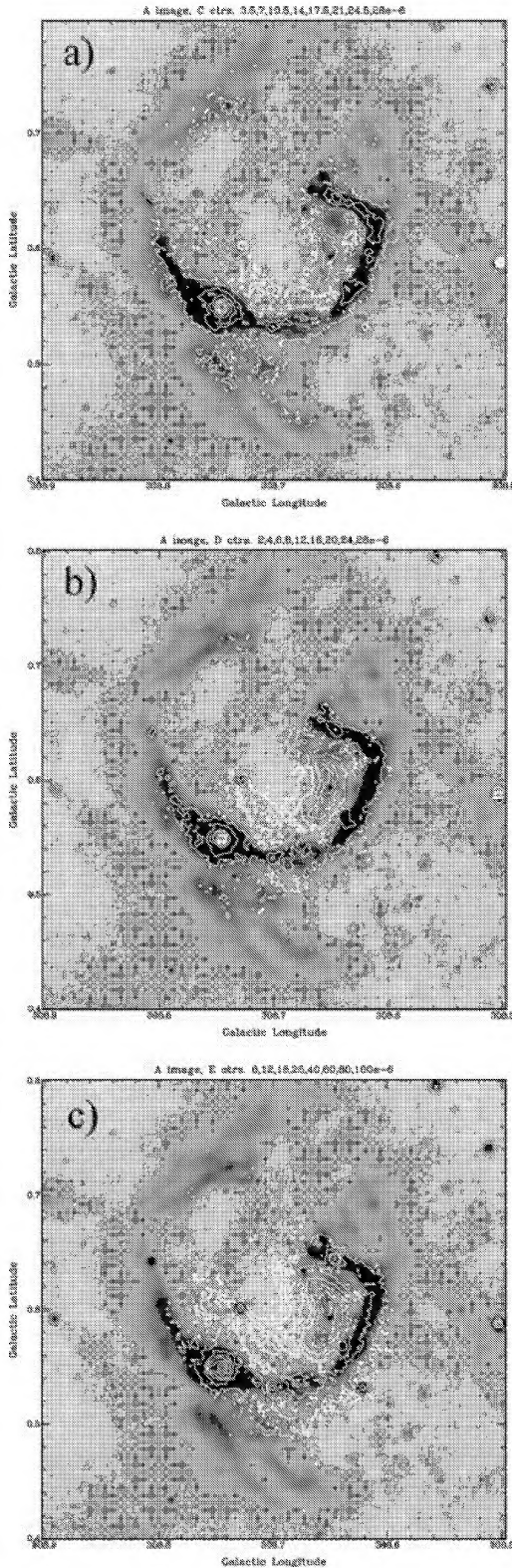


Figure 10. Linear, grey-scale, 8.3- μm image of G308.70 + 0.60 overlaid by (a) 12.1- μm (white) contours for values of 3.5, 7, 10.5, 14, 17.5, 21, 24.5, $28 \times 10^{-6} \text{ W m}^{-2} \text{ sr}^{-1}$; (b) 14.6- μm (white) contours for 2, 4, 6, 8, 12, 16, 20, $24 \times 10^{-6} \text{ W m}^{-2} \text{ sr}^{-1}$; (c) 21.3- μm (white) contours for values of 6, 12, 18, 25, 40, 60, 80, $100 \times 10^{-6} \text{ W m}^{-2} \text{ sr}^{-1}$.

One cool dust feature is the crescent which fits neatly inside the bright, PAH-emitting ring on the western side. An estimate of the temperature of these grains can be obtained by spatial integration of the crescent's radiance distributions at all four bands, which are converted to the monochromatic flux densities $<5.9, 4.7, 19.5$ and $121 \times 10^{-17} \text{ W cm}^{-2} \mu\text{m}^{-1}$ at 8.3, 12.1, 14.6 and 21.3 μm , respectively. From these results we derive a dust temperature of $\sim 85 \text{ K}$, assuming optically thick grains. Such a temperature would have a peak flux consistent with the brightness of the southern portions of the ring in the *IRAS* 60- and 100- μm images.

A similar MIR continuum-emitting feature is the quasi-linear structure inside the bright ring in the south as seen in Figs 1(d), 10(b) and (c). The SED of this triangular wedge of MIR emission suggests thermal emission by blackbody grains at a temperature close to 100 K, on the basis of the detections at 12.1, 14.6 and 21.3 μm . PAH molecules do not appear to contribute significantly to this structure.

Another intriguing aspect of G308.70 + 0.60 is the pair of parallel curving MIR filaments extending from the southern edge of the ring. These are conspicuous structures only at 8.3 μm , weak at 12.1 μm , and essentially absent at 14.6 and 21.3 μm , which suggests PAH emission. They are also seen in the 843-MHz continuum but are not resolved (Figs 4 and 5). In $\text{H}\alpha$ (Fig. 4), very faint emission overlies one of these paired filaments and extends from the south rim to the west of these filaments, but there are no counterparts in the corresponding UKST red-continuum image. An 8.3- μm curving filament, centred to the west near (308.52, +0.58) (Fig. 10), gives the impression of a partial secondary bubble, perhaps caused by leakage of UV photons from the main ring, and possibly associated with this faint $\text{H}\alpha$ emission.

4 RED SPECTROSCOPY OF G308.70 + 0.60 WITH SPIRAL

On 2001 January 4, the Anglo-Australian Observatory's (AAO) Integral Field Unit 'SPIRAL' (Lee & Taylor 2000) was used on the AAO 3.9-m telescope. During this very early post-commissioning run we had the opportunity to obtain spectra at three locations (a, b and c) in the brightest portions of the SuperCOSMOS digitized $\text{H}\alpha$ image (Fig. 11). The observed spectral range was 6350–7600 \AA at a resolution of 3 \AA ($1.2 \text{ \AA pixel}^{-1}$) in 1.5-arcsec seeing (all wavelengths from SPIRAL are given in angstroms). The averaged LSR velocities and densities derived from the major nebular lines ([N II] $\lambda 6548/6583$, $\text{H}\alpha$, [S II] $\lambda 6717/6731$, [A III] $\lambda 7135.8$) are summarized in Table 1. Our objective was to secure adequate signal-to-noise ratio spectra of three different patches of extended, low-surface-brightness, $\text{H}\alpha$ emission. The integrated spectrum for each patch is shown in Fig. 12 and represents the sum of individual spectra from 150 fibres (each 2 arcsec in diameter). There appears to be a host of other night-sky lines beyond $\lambda 7200$ which were identified as such from separate night-sky exposures during a subsequent observing run with SPIRAL. No other lines beyond $\lambda 7200$ were unambiguously attributed to G308.70 + 0.60. Therefore, Fig. 12 presents the SPIRAL spectra only between 6330 and 7200 \AA .

In order to investigate the internal velocity structure of the ring and characterize the nature of the nebula (reflection, emission, shock, etc.), we compared our derived LSR velocities (see Table 1) with published radio recombination line observations. The velocity determined for the average of the spectra in the three positions we observed is $v_{\text{LSR}} = -55 \pm 4 \text{ km s}^{-1}$. Statistically we find no significant velocity differences between regions a, b, c and those velocities

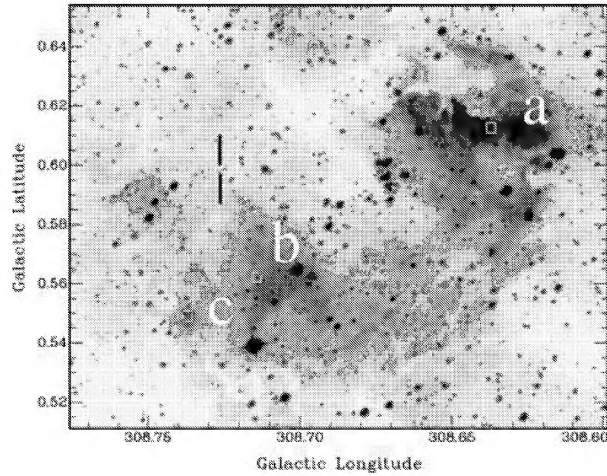


Figure 11. The three nebular locations where SPIRAL spectra were obtained are shown by open squares plotted at their actual sizes in this deep $H\alpha$ image. Between the black vertical bars lies the likely optical counterpart to the star seen in the MIR images. The picture is from a SuperCOSMOS scan of the $H\alpha$ image of this region.

found in the literature, although there is perhaps marginal ($<2\sigma$) evidence for a smaller blueshift of the gas in position **c**.

The ratios of the intensities of the red [S II] lines indicate very similar densities in positions **a** and **c**, but a much lower density in **b**, in the triangle of faint $H\alpha$ emission. In position **c**, close to the star on the rim, the [S II]/ $H\alpha$ ratio is three to five times larger than elsewhere, indicating either a much lower excitation spectrum or perhaps an additional component of $H\alpha$ emission not present elsewhere. All three locations have the basic spectral character of an H II region. There is little or no difference in either line-width or velocity in the three locations, hence there is no indication of substantial internal gas motions causing turbulence or pressure broadening within the ring.

5 H I AND CO DATA CUBES

A data cube from the H I southern sky survey (McClure-Griffiths et al. 2001) containing G308.70+0.60 was kindly prepared for us by McClure-Griffiths (private communication). The spatial resolution was 40 arcsec and the velocity spacing was 0.82 km s^{-1} . A search was made over a wide velocity range for H I emission associated with the PDR of G308.70 + 0.60 and with IRAS 13 374–6130. No unambiguous H I emission features matched the peripheral PDR but an obvious H I void was found for LSR velocities between -26.4 and -28.9 km s^{-1} (Fig. 13). This void is significant on the basis of a comparison with both the spatial and velocity distributions in a much wider area surrounding G308.70 + 0.60.

A ^{12}CO data cube was similarly constructed from data presented by Bronfman et al. (1989). The velocity coverage of their survey

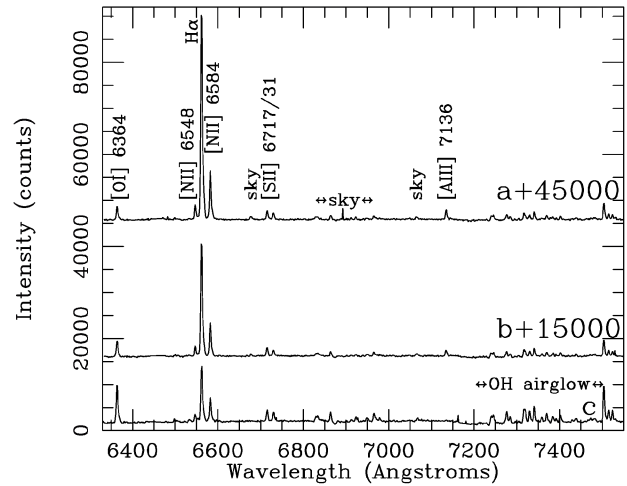


Figure 12. The three separate SPIRAL spectra, from top to bottom: positions **a**, **b**, **c**. The two upper spectra are shown displaced vertically for clarity by the amounts indicated above the red end of each spectrum. The spectra are dominated by nebular lines of $H\alpha$, [N II] and [S II]. Identifications are given for all the unequivocal nebular lines detected. Other assignments to ‘sky’ or ‘OH airglow’ emission features are shown, based on our separate night–sky spectrum.

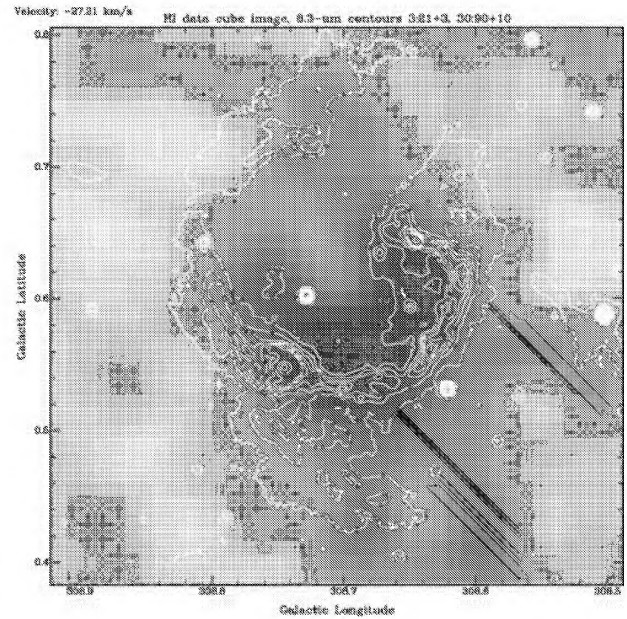


Figure 13. Grey-scale image of H I data for the LSR velocity range -27.2 km s^{-1} . White lines represent the PDR at $8.3 \mu\text{m}$ with a more detailed set of contours than those of Fig. 2. The void is apparently associated with the interior of G308.70 + 0.60.

Table 1. Observations with SPIRAL.

Location	RA 2000			Dec. 2000			GLON	GLAT	Exposure	Velocity	N_e [S II]
	h	m	s	°	'	''					
a	13	39	56.00	-61	43	08.9	308.643	0.614	100	-56 ± 4	220
b	13	40	35.39	-61	45	11.7	308.713	0.566	100	-61 ± 4	10:
c	13	40	51.53	-61	45	17.2	308.744	0.558	200	-46 ± 8	170

is -166 km s^{-1} to $+166 \text{ km s}^{-1}$ with a sensitivity of 0.1 K rms at $\delta v = 1.3 \text{ km s}^{-1}$. The spatial resolution was 8.8 arcmin . For $0^\circ:0 \leq |b| \leq 0^\circ:75$, the sampling interval is $0^\circ:125$ and for $0^\circ:75 < |b| \leq 2^\circ:0$, the sampling interval is $0^\circ:25$.

The only molecular emission near G308.70 + 0.60 occurs in the general vicinity of IRAS 13 374–6130, for LSR velocities between -47.5 and -44.9 km s^{-1} . The low spatial resolution of the CO cube precludes any strong statement as to the presence of molecular gas in the interior of the major ring. However, over a wide region, the sole area containing significant CO emission includes both IRAS 13 374–6130 and the region immediately south-east of this source.

The average optical nebular velocity is in excellent agreement with the velocities derived from the ^{12}CO data, the CS 2–1 line, the methanol masers, and the radio recombination lines measured in two locations within G308.70 + 0.60. We conclude that the major ring H II region of G308.70 + 0.60 proper is associated with MIR, H α , and radio continuum emission, lies at a distance of $5.3 \pm 0.4 \text{ kpc}$ from the sun, and its south-eastern wall has encountered a dense molecular cloud, likely to have caused secondary star formation associated with IRAS 13 374–6130 and its ultracompact H II region.

6 WHERE IS THE EXCITING STAR OF G308.70 + 0.60?

G308.70 + 0.60 appears to be a classical H II region from the morphology of its radio and MIR continuum emission. The outer PDR consists of clumpy filaments at $8.3 \mu\text{m}$, which emission we attribute to PAH bands. The exciting star of this H II ring should be detectable.

The most plausible candidate for the exciting star is located near the centre of the ring, at $l = 308^\circ:728$, $b = 0^\circ:601$. It can be seen clearly at 8.3 , 12.1 and $14.6 \mu\text{m}$ (Figs 1a, b, and c), and faintly at $21.3 \mu\text{m}$ (Fig. 1d). It is in fact the only significant MIR point source internal to the ring seen in all four *MSX* bands. In all the MIR images, except that at $8.3 \mu\text{m}$, there is an interesting counterpart to the H α structure at location **b** (Fig. 11), which has a triangular morphology (see Fig. 10). Indeed, in Fig. 7 one sees a striking piece of circumstantial evidence that apparently associates the potential exciting star with the H α and MIR nebulosity. The same ‘pointer’ is also seen at 12.1 and $14.6 \mu\text{m}$. The bright western side of this triangular nebulosity corresponds to the quasi-linear MIR feature described in Section 3.3, and is quite obvious in Fig. 1.

The SED of this star within the ring has been calculated. Fig. 14 presents the observed data (filled squares with $\pm 3\sigma$ error bars) from 0.5 to $21.3 \mu\text{m}$ in a logarithmic (λ , F_λ) plot. The short-dashed line, ‘FF’, corresponds to optically thin free–free emission, according to $F_\lambda \propto \lambda^{-2}$. This mechanism characterizes the IR emission from luminous stars with winds, such as OBA supergiants and Of stars (Barlow & Cohen 1977), and non-dusty Wolf–Rayet stars (WRs: Cohen, Barlow & Kuhl 1975). WRs show the greatest perturbations to their SEDs due to their large mass loss rates (a few $\times 10^{-5} M_\odot \text{ yr}^{-1}$), with free–free emission detectable above the stellar photospheres at 1.6 or $2.2 \mu\text{m}$. However, Of stars ($\dot{M} \sim \text{few} \times 10^{-7} M_\odot \text{ yr}^{-1}$) show free–free at 3.6 and even $2.2 \mu\text{m}$ in some cases, while OBA supergiants ($\dot{M} \sim \text{few} \times 10^{-6} M_\odot \text{ yr}^{-1}$) show this emission process at $\sim 10 \mu\text{m}$.

Table 2 lists the isophotal wavelengths and flux densities that define the SED of this potential exciting star for the ring.

An estimate of the minimum bolometric luminosity of the exciting star is important. A strictly lower bound corresponds simply to integration under the observed SED, with the minimum-luminosity extrapolation beyond $21.3 \mu\text{m}$, and yields $19\,000 L_\odot$. Clearly, the intervening reddening of this star severely affects any estimate of

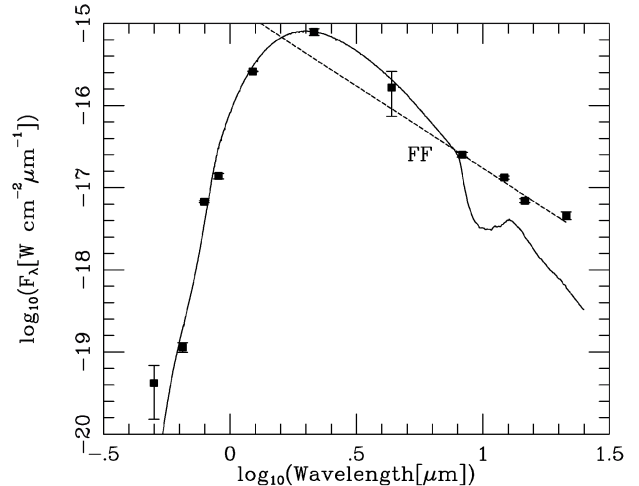


Figure 14. The observed SED of the potential exciting star of G308.70 + 0.60 defined by UKST optical, DENIS near-infrared, and the *MSX* observations. 3σ absolute error bars are shown. ‘FF’ indicates the slope of the intrinsic spectrum of optically-thin free–free emission, normalized to the $8.3\text{-}\mu\text{m}$ flux density. The solid curve with the deep silicate absorption feature near $10 \mu\text{m}$ represents the Kurucz synthetic spectrum of an O6V star.

Table 2. Observed flux densities of the putative exciting star at different wavelengths.

Filter	λ_{iso} μm	F_λ $\text{W cm}^{-2} \mu\text{m}^{-1}$
<i>B_J</i>	0.50	4.18E-20
<i>R</i>	0.65	1.14E-19
<i>I</i>	0.90	1.38E-17
<i>I</i> (DENIS)	0.79	6.75E-18
<i>J</i> (DENIS)	1.23	2.58E-16
<i>K_s</i> (DENIS)	2.15	$\geq 7.85\text{E-}16$
Band- <i>B₁</i>	4.36	1.66E-16
Band- <i>A</i>	8.28	2.51E-17
Band- <i>C</i>	12.13	1.33E-17
Band- <i>D</i>	14.65	6.95E-18
Band- <i>E</i>	21.34	4.59E-18

its luminosity. If we redden the SED of an OB-star (represented by a Kurucz model spectrum) with $A_V \sim 20$, the fit to the observations (Fig. 14, solid curve) is remarkably good at wavelengths below $12.1 \mu\text{m}$. The Kurucz SED shown corresponds to an O6V, but an equally heavily reddened O8I’s SED also fits the observed SED. Such stars have an $L_{\text{bol}} \sim 400\,000\text{--}550\,000 L_\odot$ (Panagia 1973), a luminosity entirely consistent with a Wolf–Rayet star too.

The combination of such a highly extinguished hot star with an apparently unperturbed MIR free–free slope suggests that the extinction is local to the star, most likely in an edge-on circumstellar disc, so that the star is reddened but the much more extensive volume containing the stellar wind is not.

If we estimate the radius of the Stromgren sphere surrounding this candidate exciting star, R_s , it is $\sim 8 \text{ pc}$. To deduce the excitation parameter, U , for the star we need an estimate for the spatially averaged product of $R_s (N_e N_H)^{1/3}$. From the SPIRAL [S II] line ratios one might expect $N_e N_H \sim 100\text{--}1000$, though this clearly depends on the ionization fraction of the gas, from which $U \sim 0.1\text{--}0.2 R_s$, or $U \sim 40\text{--}80 \text{ pc cm}^{-2}$. This requires that the exciting star lies in the range of spectral types O6–O8.5V, if a main sequence star, or O8–B0I, if a supergiant (Panagia 1973). Its mass would be

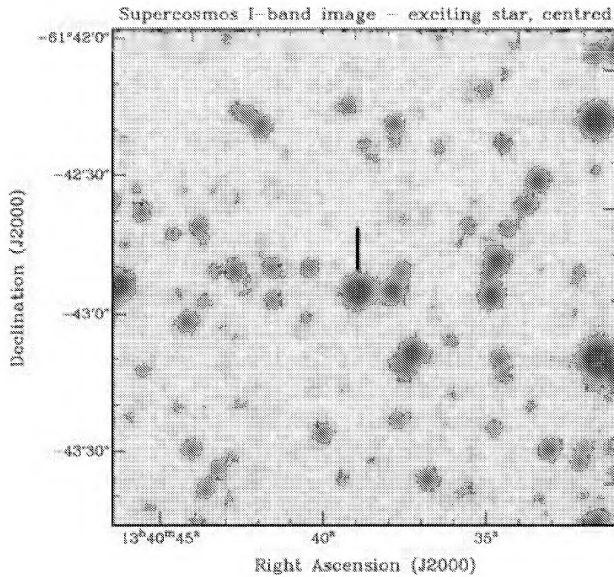


Figure 15. *I*-band SSS image of the possible exciting star, which is located at the centre of the image. The black bar indicates the optical counterpart of the MIR source.

at least $\sim 30 M_{\odot}$. Similarly, a Wolf–Rayet star could provide this luminosity and ionizing flux.

The median diameter of a sample of 40 optical nebulae around southern WR stars (Marston 1997) is 12 pc. Segregated by type of bubble his sample shows median diameters of 7 pc (for WR-phase wind-blown), 12.5 pc (mass-loss ejecta phase), and 37.5 pc (radiative coupling from the O-star wind-blown phase). G308.70 has a diameter of 16 pc, half the median size if it were caused by an O-star wind, but twice as large as the median for bubbles attributable to the wind of a WR star. The presence of the MIR free-free emission from a stellar wind would be consistent with either a late O-supergiant (Barlow & Cohen 1977), or a WR with a wind but no dust (i.e. a WN or WCE type: Cohen et al. 1975). Only an optical stellar spectrum could definitively determine which.

The deep $H\alpha$ image (Fig. 11) shows a faint stellar object apparently at the same position as the $8.3\text{-}\mu\text{m}$ point source (J2000 RA $13^{\text{h}}40^{\text{m}}39^{\text{s}}.42$, Dec. $-61^{\circ}42'56''.5$, shown between the black tick marks). The B_J -, R - and I -band photometry in Table 2 is that returned using SuperCOSMOS IAM data for the source, taken from the on-line SuperCOSMOS Sky Surveys (SSS).² Fig. 15 presents a portion of the I plate that identifies the optical counterpart (at J2000 RA $13^{\text{h}}40^{\text{m}}39^{\text{s}}.33$, Dec. $-61^{\circ}42'51''.7$), within 5 arcsec of the MIR source. The object is extremely red: $B_J = 20.11$, $R = 18.20$, $I = 12.02$, whence $B_J - R = 1.9$, $R - I = 5.3$. *IRAS* images at 60 and $100\ \mu\text{m}$ do not have the spatial resolution to distinguish this star from the bright FIR emission that fills all the southern portion of the main ring. The DENIS point source archives reveal a near-infrared object at J2000 RA $13^{\text{h}}40^{\text{m}}39^{\text{s}}.42$, Dec. $-61^{\circ}42'51''.8$, with $I = 13.09$, $J = 7.72$, $K \leq 4.36$ (the latter is saturated), only 5 arcsec from the MIR source.

This choice of object for the exciting star is plausible because it sits on the edge of the H I void and could have photo-evaporated away all trace of local extended CO/MIR/ $H\alpha$ emission with its UV radiation. The diffuse *IRAS* 60 and $100\text{-}\mu\text{m}$ emission within G308.70 + 0.60 would correspond to emission by cool dust grains,

² Available at <http://www-wfau.roe.ac.uk/sss/>.

powered by dilute starlight, outside the H I void. The exciting star, and much of the dense obscuration apparent at optical wavelengths would lie in the front portion of the bubble, expanding at $\sim 20\ \text{km s}^{-1}$ toward us, that we see projected and limb-brightened as the outer ring of G308.70 + 0.60. The H I void would have been caused by the complete dispersal of gas on the far side of the bubble by the stellar wind. We speculate that the major breakout (see below) on the north-west rim, and the long tendrils of $8.3\text{-}\mu\text{m}$ emitting gas that extend to the north of G308.70 + 0.60 (see Fig. 1a), represent the direction in which the original H I gas was driven before losing its identity in the ISM. In the opposite direction, the bipolar stellar wind encountered the dense molecular gas outside the south-east rim and the foreground obscuring gas and dust, and the complete dispersal of blueshifted H I gas was prevented.

We, therefore, suggest that the star is embedded in a substantial circumstellar shell within which there lies an equatorial toroid, viewed somewhat close to edge-on, of sufficient density and mass to confine the stellar wind to lie along an axis roughly in position angle 150° – 330° , and produce substantial reddening of the exciting star itself.

7 CONCLUSIONS

It is feasible that our suggested source is more than capable of generating the bubble of G308.70 + 0.60. Its non-central position within the overall ring is explained by the substantially higher local density beyond the bright south-eastern wall than that outside the northern rim, where the outer PDR is incomplete and of much lower brightness. It is possible that the northern breakout through the outer PDR is a consequence of the low (or decreasing) ambient density outside the ring at greater Galactic latitude. It is also interesting that the axis of this break in the bubble is collinear with the potential exciting star and with *IRAS* 13 374–6130. This breakout does not signify an absence of ionized gas since both $H\alpha$ emission and some 843-MHz emission (Fig. 3) are apparent in the gap in the PDR. In fact, Fig. 3 shows that the radio continuum traces the entire bubble although the thermal emission is somewhat less intense in the breakout. A second, smaller breakout occurs in the east rim near (308.80, +0.68), and might have produced the small, bright nebulosity at (308.90, +0.70).

There is an excellent match between the radio continuum and $H\alpha$ morphologies over the entire ring, including within the bright triangular $H\alpha$ patch, **b**. Therefore, it is reasonable to interpret locations within the main ring where $H\alpha$ is weak (e.g. at the very centre, $l = 308.69$, $b = 0.62$) as due to obscuration by overlying cold dust. There is little $21.3\text{-}\mu\text{m}$ emission from the centre, but the interior of the bubble is filled with *IRAS* 60- and $100\text{-}\mu\text{m}$ emission, suggesting that internal low-temperature dust may cause much of the overlying extinction. At the position of the exciting star there is also an indication of overlying dust but it cannot be determined at present if this dust is inside the H II region or in the immediate circumstellar vicinity of the exciting star. However, there is no prominent $10\text{-}\mu\text{m}$ silicate absorption in the SED of the potential exciting star (e.g. a depressed $8.3\text{-}\mu\text{m}$ flux density compared with that at $12.1\ \mu\text{m}$), which implies little extinction through the edge-on plane of any disc, along our line-of-sight to the star. We speculate that the $H\alpha$ wedge of emission (**b**) south of the star is due to light scattering out through a hole in the encompassing circumstellar dust cloud. The western edges of the triangular $H\alpha$ patch and the $21.3\text{-}\mu\text{m}$ pointer lie in approximately the same position angle, so the same escaping stellar radiation ionizes local gas and heats local dust grains.

In the logarithmic intensity plots of G308.70 + 0.60 at $8.3\ \mu\text{m}$ (Fig. 1) and 843 MHz (Fig. 5), there is essentially no detectable

emission in the main bubble. The brightness of the walls can be explained by limb-brightening at both frequencies but it is peculiar that the interior should be so empty compared with the brightness of the ambient medium (Fig. 6). An extinction, A_V , of order 3 mag caused by dust internal to the ring could explain the 8.3- μm dimming and such dust grains might locally be sufficiently numerous to compete with gas for ionizing photons, thereby diminishing the 843-MHz free-free brightness.

If we apply the same technique of treating the arc nebula around IRAS 13 374–6130 as a Stromgren sphere as we did for the exciting star of the major ring, then we find: $R_s \sim 0.9$ pc, $N_e N_H \sim 30$ (from Table 1 for the density at position c). Consequently, the excitation parameter for the star powering IRAS 13 374–6130 would be ~ 27 , suggestive of an O9.5V with bolometric luminosity 66 000 L_\odot (Panagia 1973), very close to our previous estimate for the minimum luminosity required to power the region around IRAS 13 374–6130 (Section 3.1).

Further candidates for secondary star-forming regions can be identified on, or within, the rim of the major ring by their 21.3- μm brightness, colour indices between the *MSX* bands (all are suggestive of compact H II regions), and absence of coincident H α emission (indicating heavily obscured regions). Four of these (see Fig. 1d) lie at (308.646, +0.644), (308.639, +0.569), (308.701, +0.532) and (308.688, +0.526), but all are far fainter than IRAS 13 374–6130. Their minimum bolometric luminosities are between 1300 and 2500 L_\odot , indicative of at least B3–B4V stars.

Further star formation may also be occurring within the patch of intense H α (region a, Fig. 11), which is also seen at 8.3- μm , and in radio continuum, just inside the west rim of the ring of G308.70 + 0.60. Extremely heavy obscuration north of the crescent has led to ‘elephant trunk’ structures in the interface between dust and ionized gas (Fig. 11, at 308.65, +0.62). No MIR point sources are detected by *MSX* within this dense dusty region. The various *IRAS* catalogues do not suggest any embedded, still-forming, high-mass stars in the far-infrared but this may be in part due to the brightness of the diffuse emission associated with the interior of the whole major ring.

To appreciate the complex structure of G308.70 + 0.60 and the manner in which it interacts with its surroundings we return to Fig. 1(a), which represents a stretched, high-contrast, unsharp-masked, negative version of the 8.3- μm image. This high-contrast image clearly shows: the way that the PDR around G308.70+0.60 is revealed to consist of many overlapping filaments rather than a single continuous structure [in keeping with the findings of Cohen & Green (2001) for a wide variety of H II regions compared in *MSX* MIR and MOST radio continuum imagery]; the contiguous secondary bubble outside the south-western rim; a curious stubby bright filament slightly displaced from, and orthogonal to, the eastern rim; and the long, faint northern filament with its cap of emission, possibly driven by a stellar wind passing through the north-western ‘breakout.’ Perhaps the most enigmatic feature associated with G308.70 + 0.60 is the apparently conical structure (Fig. 1) whose apex lies just inside the bright south-eastern wall and whose divergent end passes through (seemingly in front of) the north-western breakout. The surface of this conical wind is apparently covered along its length by a lattice of rather regularly spaced faint filaments. We speculate that these might represent a series of bowshocks, produced by episodic mass-losing events in the exciting star.

ACKNOWLEDGMENTS

We acknowledge Sebastian Juraszek for assistance with the initial radio/MIR comparisons. We thank Thomas Dame for his suggestion

that, for small-scale studies, the use of the individual surveys cited in his ‘New Complete CO Survey’ would best suit our needs, Jim Caswell for sharing unpublished data on methanol masers and for valuable discussions, and Guy Simon for extracting the DENIS point source photometry for our candidate exciting star. MC thanks NASA for supporting this work under its Long Term Space Astrophysics programme, through grant NAG5-7936. The MOST is owned and operated by the School of Physics, within the University of Sydney, supported by the Australian Research Council and the University of Sydney. The AAO is undertaking the H α survey on behalf of the astronomical community.

REFERENCES

- Barlow M. J., Cohen M., 1977, *ApJ*, 213, 737
 Bock D. C.-J., Large M. I., Sadler E. M., 1999, *AJ*, 117, 1578
 Bronfman L. H., Cohen R. S., Thaddeus P., 1989, *ApJS*, 71, 481
 Bronfman L., Nyman L.-A., May J., 1996, *A&AS*, 5, 81
 Caswell J., 2001, *MNRAS*, 326, 805
 Caswell J. L., Haynes R. F., 1987, *A&A*, 171, 261
 Chavarria C. K., 1981, *A&A*, 101, 105
 Cohen M., 1973, *MNRAS*, 164, 395
 Cohen M., 1994, *AJ*, 107, 582
 Cohen M., Green A. J., 2001, *MNRAS*, 325, 531
 Cohen M., Barlow M. J., Kuhl L. V., 1975, *A&A*, 40, 291
 Cohen M., Walker R. G., Witteborn F. C., 1992, *AJ*, 104, 2030
 Egan M. P. et al., 1999, *The Midcourse Space Experiment Point Source Catalog Version 1.2 Explanatory Guide*. Air Force Research Laboratory Technical Report, AFRL-VS-TR 1999–1522
 Fich M., Blitz L., Stark A. A., 1989, *ApJ*, 342, 272
 Green A. J., 1999, in Landecker T., Taylor R., eds. *ASP Conf. Ser. Vol. 168, New Perspectives on the Interstellar Medium*. Astron. Soc. Pac., San Francisco, p. 43
 Green A. J., Cram L. E., Large M. I., Ye T., 1999, *ApJS*, 122, 207
 Lee D., Taylor K., 2000, in Iye M., Moorwood A. F., eds. *Optical and IR Telescope Instrumentation and Detectors*. Proc. SPIE Vol. 4008, p. 268
 Marston A. P., 1997, *ApJ*, 475, 188
 McClure-Griffiths N. M., Green A. J., Dickey J. M., Gaensler B. M., Haynes R. F., Wieringa M. H., 2001, *ApJ*, 551, 394
 Mill J. D. et al., 1994, *J. Spacecraft Rockets*, 31, 900
 Miller L., Cormack W., Paterson M., Beard S., Lawrence L., 1992, in MacGillivray H. T., Thomson E. B., eds. *Digitised Optical Sky Surveys*. Kluwer, Dordrecht, p. 133
 Mills B. Y., 1981, *Proc. ASA*, 4, 156
 Panagia N., 1973, *AJ*, 78, 929
 Parker Q. A., Bland-Hawthorn J., 1998, *PASA*, 15, 33
 Parker Q. A., Malin D., 1999, *PASA*, 16, 288
 Parker Q. A., Phillips S., 2001, in Clowes R., Adamson A., Bromage G., eds. *ASP Conf. Ser. Vol. 232, The New Era of Wide Field Astronomy*. Astron. Soc. Pac., San Francisco, p. 38
 Parker Q. A., Phillips S., Morgan D. H., 1999, in Taylor A. R., Landecker T. L., Joncas G., eds. *ASP Conf. Ser. Vol. 168, New Perspectives on the Interstellar Medium*. Astron. Soc. Pac., San Francisco, p. 126
 Price S. D., Egan M. P., Carey S., Mizuno D., Kuchar T., 2001, *AJ*, 121, 2819
 Reid M. J., Ho P. T. P., 1995, *ApJ*, 288, L17
 Robertson J. G., 1991, *Aust. J. Phys.*, 44, 729
 Roche P. F., Aitken D. K., 1984, *MNRAS*, 208, 481
 Van Buren D., Noriega-Crespo A., Dgani R., 1995, *AJ*, 110, 2914
 Van Der Walt D. J., Gaylard M. J., MacLeod G. C., 1995, *A&AS*, 110, 81
 Volk K., Cohen M., 1989, *AJ*, 98, 931
 Wilson T. L., Mezger P. G., Gardner F. F., Milne D. K., 1970, *A&A*, 6, 364
 Wood D. O. S., Churchwell E., 1989, *ApJ*, 340, 265
 Wright A. E., Griffith M. R., Burke B. F., Ekers R. D., 1994, *ApJS*, 91, 111

This paper has been typeset from a $\text{\TeX}/\text{\LaTeX}$ file prepared by the author.